Journal of Alloys and Compounds 651 (2015) 144–148

Contents lists available at ScienceDirect

Journal of Alloys and Compounds

journal homepage: http://www.elsevier.com/locate/jalcom

Permanent magnetic properties of rapidly quenched $(La,Ce)_2Fe_{14}B$ nanomaterials based on La–Ce mischmetal

Ming Zhang [a], Zhubai Li [b], Baogen Shen [a, *], Fengxia Hu [a], Jirong Sun [a]

[a] State Key Laboratory for Magnetism, Institute of Physics, Chinese Academy of Sciences, Beijing, 100190, China
[b] Key Laboratory of Integrated Exploitation of Bayan Obo Multi-Metal Resources, Inner Mongolia University of Science and Technology, Baotou, 014010, China

ARTICLE INFO

Article history:
Received 15 February 2015
Received in revised form
5 August 2015
Accepted 6 August 2015
Available online 8 August 2015

Keywords:
Permanent magnets
Mischmetal
Rapid-solidification
Magnetic properties

ABSTRACT

High performance $(La_{0.35}Ce_{0.65})_xFe_{14}B$ (x = 2.0, 2.4, 2.8, 3.2, 3.6, 4.0) ribbons were prepared by melt-spinning method, using industrial La–Ce mischmetal. Phase composition and room temperature permanent magnetic properties were investigated. The main phases of all samples crystallize in the tetragonal 2:14:1 type structure. A second-phase appears when x = 3.6 and 4.0, which is La–Ce alloy with a crystal structure of face-centered cubic but not $CeFe_2$. Replacement of $CeFe_2$ by La–Ce alloy enhances the temperature stability of the magnetic material at low temperature. The intrinsic coercivity increases with x monotonously, and the energy product reaches a maximal value of 8.29 MGOe at x = 2.4 when an optimal wheel velocity of 20 m/s was adopted, which is twice of that of $Ce_2Fe_{14}B$. The coercivity mechanism and intergrain exchange coupling were studied by using minor loops. The results indicated that strong pinning effect dominate the magnetization reversal process in all of the rare-earth-rich ribbons. The structure-property relationship was analyzed by using Henkel plots, and intergrian exchange coupling were found in all samples.

1. Introduction

Since NdFeB magnet was invented in 1980s' [1,2], almost all kinds of rare-earth elements, especially light rare-earth [3,4] and mischmetals, have been used to fabricate permanent magnets. However, most of the investigations about La or/and Ce-based permanent magnets focused on their intrinsic properties, the coercivity and energy product were seldom referred. Recently, with the rising price of neodymium, a growing number of efforts have been made to fabricate permanent magnets with both high light rare earth content and outstanding properties. Two methods were applied, one is substitution [5–8], and the other is to enhance the coercivity and energy product of Ce-based permanent magnets [9–11].

Despite their name, rare-earth elements are not truly rare geologically, but they are expensive due to the extraction process [12]. Rare earth elements are extracted from associated ore. Bastnaesite ore from Bayan Obo mainly contains light rare earth elements. The so-called La–Ce–Pr–Nd mischmetal with 26–29 wt% La, 49–53 wt% Ce, 4–6 wt% Pr, and 15–17 wt% Nd is the extract of it. This La–Ce–Pr–Nd combination of metals can also be separated into La–Ce Alloy, which contents 35 wt% La and 65 wt% Ce as we used in this experiment, and Pr–Nd alloy during extraction process. Further extraction and purifying process are required to obtain pure metal La, Ce, Pr and Nd. Nowadays, a growing number of consumption of $Nd_2Fe_{14}B$ magnets resulted in an exhaustive exploitation of Nd and Pr, which have caused the overstock of La and Ce at the same time. Therefore, to fabricate $R_2Fe_{14}B$-type magnets by utilizing La or/and Ce is highly beneficial to utilize the rare-earth resource in a balanced manner and manufacture low-cost magnets. Herbst et al. studied cerium-based permanent magnets [9], and the reported energy product can be as high as 4.1 MGOe. Industrial La–Ce mischmetal shows price advantage compared to the pure metal Ce. To synthesize $R_2Fe_{14}B$-type magnets with industrial La–Ce mischmetal, and study the permanent magnetic properties should be of high significance for practical applications.

2. Experimental

The $(La_{0.35}Ce_{0.65})_xFe_{14}B$ ingots with x = 2.0, 2.4, 2.8, 3.2, 3.6 and 4.0 were prepared by arc melting technique in an argon atmosphere of high purity. The purity of starting materials is 99.9% for Fe and 96% for Fe–B alloys. Industrial mischmetal containing about 35wt%

* Corresponding author.
E-mail address: shenbg@iphy.ac.cn (B. Shen).

http://dx.doi.org/10.1016/j.jallcom.2015.08.044

La and 65wt% Ce with purity about 99.37 was used in this experiment. Table 1 lists the content of elements measured by ICP-OES in weight percentage. Considering the atomic weight of La and Ce, the atomic percentage of La is about 34.7 at% and Ce 65.1 at%, thus the chemical formula $La_{0.35}Ce_{0.65}$ was used to show the nominal composition. Pure metal Ce with the purity of 99.9wt% were used to fabricate the contrast sample $Ce_{17}Fe_{78}B_6$. All buttons were re-melted at least five times to ensure homogeneity. The ribbons were obtained directly by induction melting the precursor ingot in a quartz tube and then ejecting onto a surface of a copper wheel with a surface velocity in a range of 10–30 m/s. X-ray diffraction measurements on the as-cast and ribbon samples were performed using Cu Kα radiation to determine the crystal structure. Magnetic properties at room temperature were measured by vibrating sample magnetometer (VSM) with a maximum magnetic field of 20 kOe. The applied field is parallel to the plane of ribbons and no demagnetization correction for the geometry of the sample was made, because the demagnetization factor is nearly 1. The morphologies were studied by transmission electron microscopy (TEM).

3. Results and discussion

For ribbons prepared by melt-spinning technique, their phase formation, grain size and permanent magnetic properties are found to be strongly dependent on the wheel velocity. Fig. 1 displays the X-ray diffraction pattern of $(La_{0.35}Ce_{0.65})_2Fe_{14}B$ ribbons prepared in different wheel velocities. One can find that $R_2Fe_{14}B$ phase can be formed for a variety of wheel velocities, and even the as-cast sample contains mainly $R_2Fe_{14}B$ phase. Alteration of wheel velocity brings about a difference of grain size and an appearance of amorphous phase. An appropriate grain size is beneficial to enhance the coercivity and squareness of demagnetization curve. However, the appearance of too much amorphous phase will lead to a decoupling effect resulting in a decrease of energy product for isotropic magnets. Fig. 2 shows the hysteresis loops of $(La_{0.35}Ce_{0.65})_2Fe_{14}B$ ribbons prepared in different wheel velocities compared with the as-cast samples. One can notice that the coercivity enhances with the rise of wheel velocity until 20 m/s, while the as-cast sample with coarse grains possess the lowest coercivity. A velocity of 25 m/s or higher lead to the appearance of too much amorphous phase and a separation of magnetic phases, which is consistent with the results derived from XRD. Both XRD patterns and hysteresis loops indicate that the optimum wheel velocity for $(La_{0.35}Ce_{0.65})_2Fe_{14}B$ is about 20 m/s where the coercivity and energy product reach their largest value simultaneously. $(La_{0.35}Ce_{0.65})_2Fe_{14}B$ ribbons prepared at a velocity close to 20 m/s (such as 18 m/s and 22 m/s) were also carried out. We found the magnetic properties, which are not shown here, are almost the same with the sample that prepared at 20 m/s. It means that the magnetic properties of the mischmetal-based magnetic ribbons prepared by melt-spinning are less sensitive to the wheel velocity around 20 m/s compared to the case of $Nd_2Fe_{14}B$, indicating the former possesses a broadening optimum velocity range. A high tolerance for process parameters is an attractive advantage in mass production.

Ribbons were also prepared in different wheel velocities for other compositions, and the optimal velocities are around 20 m/s for almost all compositions involved in present work. The dependence of magnetic properties on rare earth contents was studied and samples selected here are all prepared in a velocity of 20 m/s.

Table 1
Contents and impurities of the Mischmetal used in this experiment.

REM	La/TREM	Ce/TREM	Pr/TREM	Nd/TREM	Fe	Si	Cu	Zn	Others
99.37	34.47	65.33	<0.05	<0.05	0.29	<0.05	<0.02	<0.30	<0.10

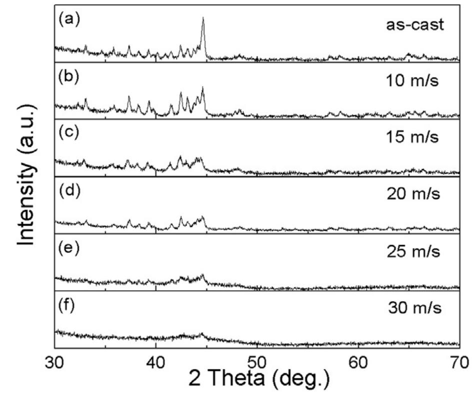

Fig. 1. The XRD patterns of $(La_{0.35}Ce_{0.65})_2Fe_{14}B$ ribbons.

X-ray diffraction patterns in Fig. 3 confirmed that $R_2Fe_{14}B$ phase is the dominant phase in all samples, and no RE-Fe binary phases or rare earth oxides was found. Early investigation [9] has shown that in $Ce_{17}Fe_{78}B_6$ the excess Ce brings a second-phase of $CeFe_2$, with a mass fraction of about 12%. Different from $Ce_xFe_{14}B$, excess rare earth in $(La_{0.35}Ce_{0.65})_xFe_{14}B$ tend to maintain its original La–Ce solid solution form. The crystal structure of La–Ce alloy was studied by using XRD. Fig. 3(g) shows that the dominant phase of La–Ce alloy is La–Ce face-centered cubic solid solution with a space group of Fm-3m, and the lattice parameter is a = 0.522 nm. The standard indexes of La and Ce with the same space group were also plotted in the figure. One can never ignore the diffraction peak at 29.6° and 34.3°, which corresponding to {111} and {200} of La–Ce alloy in the diffraction patterns of $(La_{0.35}Ce_{0.65})_{3.6}Fe_{14}B$ and $(La_{0.35}Ce_{0.65})_{4.0}Fe_{14}B$ ribbons. In consideration of the resolution limitation for XRD, SAED was carried out to clarify the absence of $CeFe_2$ and the existence of La–Ce alloy. The SAED pattern and analysis are shown in Fig. 4.

Magnetic properties may be more sensitive to $CeFe_2$. The Curie temperature of $CeFe_2$ is about 235 K, $CeFe_2$ is ferromagnetic material with low anisotropy field and high saturation magnetization below this temperature. Hence, if the samples consist of $CeFe_2$ and a kind of ferromagnetic material with high anisotropy field, such as $R_2Fe_{14}B$, an obvious drop will appear in the magnetization vs. temperature curve measured at low external field due to FM-PM transition of $CeFe_2$. The dependence of magnetization on temperature for all samples at an external field of 100 Oe is shown in Fig. 5.

Fig. 5(a) shows the dependence of magnetization on temperature of $Ce_{17}Fe_{78}B_6$ measured at 100 Oe. The insets are the hysteresis

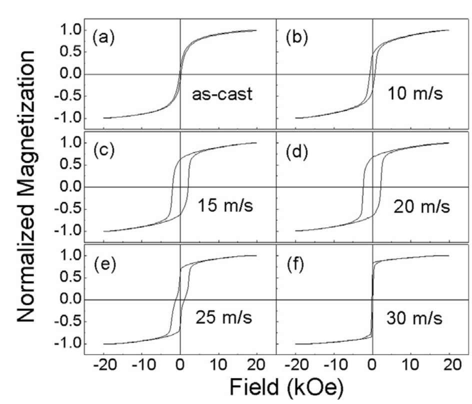

Fig. 2. The hysteresis loops of $(La_{0.35}Ce_{0.65})_2Fe_{14}B$ ribbons.

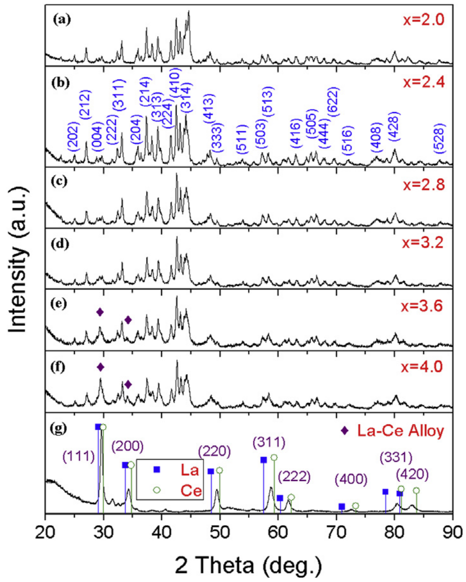

Fig. 3. The XRD patterns of $(La_{0.35}Ce_{0.65})_xFe_{14}B$ ribbons prepared at a wheel velocity of 20 m/s.

loops of $Ce_{17}Fe_{78}B_6$ measured at 150 K and 300 K. $Ce_{17}Fe_{78}B_6$, contains about 12% $CeFe_2$ phase, is the single composition yielding the best overall performance as mentioned in Ref. [9]. The magnetization drops obviously around the Curie temperature of $CeFe_2$. The hysteresis loops measured at different temperature gives more evidence. At 300 K, the sample contains only one ferromagnetic phase, which is $Ce_2Fe_{14}B$, thus the hysteresis loop shows a character of hard magnet with a single phase. At 150 K, the sample contains two ferromagnetic phases, they are $Ce_2Fe_{14}B$ and $CeFe_2$, and the magnetization drops at a low negative field is a result of moment reversal of $CeFe_2$. Fig. 5(b) shows the dependence of magnetization on temperature of all the samples in this work measured at 100 Oe. The inset is the hysteresis loops of these samples measured at 150 K. No evidence of the existence of $CeFe_2$ was found.

Fig. 6 shows the hysteresis loops of these samples. The values of B_r, H_{cj}, $(BH)_{max}$, remanence ratio, and squareness were listed in Table 2. For all the samples, the intrinsic coercivity enhances with increasing the rare-earth metal content. Both the saturation magnetization and remanence decrease due to the formation of rare-earth-rich phases. For the behavior of the maximum magnetic energy product, it is found that the $(BH)_{max}$ first increases and then decreases with x, and the maximal value of 8.29 MGOe appears at x = 2.4. It is worthwhile to note that the maximum energy product keeps large and changes slightly in a relatively wide range of rare-earth content around x = 2.4.

The sample $(La_{0.35}Ce_{0.65})_{2.4}Fe_{14}B$ prepared at a wheel velocity of 20 m/s was selected for more investigations, noting that it possesses the best comprehensive properties. From the X-ray diffraction pattern shown in Fig. 3, one can find that the dominant phase crystallized in a 2:14:1 structure, no splits appear. It means that La and Ce atoms tend to enter the same crystal lattice instead of forming $La_2Fe_{14}B$ and $Ce_2Fe_{14}B$ phase respectively.

Early studies indicated that the saturation magnetization M_s, anisotropy field H_a and Curie temperature T_c of $Ce_2Fe_{14}B$ is 11.7 kGs, 26 kOe and 424 K, respectively. $La_2Fe_{14}B$ possess higher M_s and T_c but lower H_a, which is 13.8 kGs, 530 K and 20 kOe, respectively [13]. For $(La_{0.35}Ce_{0.65})_{2.4}Fe_{14}B$ that tends to form a pseudo-ternary compound, an intermediate magnetic property is expected which were confirmed by our experiments.

The initial magnetization curve of $(La_{0.35}Ce_{0.65})_{2.4}Fe_{14}B$ shows a characteristic of pinning mechanism, where the magnetization increases slowly until the applied field exceeds the intrinsic coercivity, and then followed by a steep rise. More evidences can be given by minor hysteresis loops. Fig. 7 reveals the dependence of normalized coercivity and remanence in minor loops on the applied field, and the maximum magnetization of each loops in the first quadrant were also plotted in this figure. The inset is the original minor loops measured by VSM. Asymmetric minor loops were observed when the maximum applied field for certain minor loops is lower than the intrinsic coercivity. This phenomenon may be resulted from the pinning effect of domain wall movements during the magnetization process. The normalized coercivity increases faster than remanence, which is another evidence of the dominant role of pinning mechanism on the coercivity of $(La_{0.35}Ce_{0.65})_{2.4}Fe_{14}B$ ribbons. This measurement was also carried out among all the rare-earth- rich samples, and the results are the same.

Fig. 8 shows the Henkel plots of $(La_{0.35}Ce_{0.65})_xFe_{14}B$ ribbon prepared at a wheel velocity of 20 m/s. The remanence ratio M_r/M_s of $(La_{0.35}Ce_{0.65})_{2.4}Fe_{14}B$ ribbons is 0.68. One knows that the value of an isotropic magnet composed of uniaxial anisotropy single-domain grains without intergrain interaction is 0.5. In this experiment, a value of M_r/M_s larger than 0.5 may indicate that intergranular exchange coupling interaction is introduced by melt-spinning method. The δM curve (defined as below) has normally been used to evaluate the intergranular exchange coupling. According to Stoner-Wohlfarth theory, $I_d(H) = 1\text{-}2I_r(H)$ [14], where $I_d(H)$ is the normalized dc-demagnetization remanence as a function of the reversal field, and $I_r(H)$ is the normalized initial isothermal remanence as a function of the applied field. The difference between the two expressions has been defined to be $\delta M(H) = I_d(H)\text{-}[1\text{-}2I_r(H)]$. A positive δM is associated with a strong intergrian exchange coupling for isotropic samples consisting of uniaxial anisotropy single-domain grains while a negative value indicates a weak or no exchange coupling interaction between grains, and magnetostatic (dipolar) interaction becomes dominant. The shape of δM curve reveals the competition among exchange coupling interaction and magnetostatic interaction. Exchange coupling interaction contributes a positive constituent, while magnetostatic interaction offers a negative constituent. The magnetostatic interaction was considered existing universally, hence, a positive value should definitely mean the existence of exchange coupling interaction. As shown in Fig. 8, every sample reveals a positive peak at the field around coercivity. Different maximum values show the difference in intergrain interaction among samples, and indicate a variety of grain boundary conditions. $(La_{0.35}Ce_{0.65})_{2.0}Fe_{14}B$ ribbon contains mainly $R_2Fe_{14}B$ phase and α-Fe, the lower maximum value of δM is mainly caused by the non-uniform magnetization reversal [15] and magnetostatic interaction effect due to the existence of α-Fe. In $(La_{0.35}Ce_{0.65})_{2.4}Fe_{14}B$ and $(La_{0.35}Ce_{0.65})_{2.8}Fe_{14}B$ ribbons, with the increase of mischmetal concentration, a thin layer of rare-earth-phase may form between the main phase grains, and the grain boundary becomes smooth, hence the maximum value of δM increased due to the improvement of grain boundary conditions. More mischmetal thickens the grain boundary, but its thickness may vary. The decrease of δM peak probably results from the homogeneity breaking of grain boundary in $(La_{0.35}Ce_{0.65})_{3.2}Fe_{14}B$ ribbons. The maximum value of δM in $(La_{0.35}Ce_{0.65})_{3.6}Fe_{14}B$ and $(La_{0.35}Ce_{0.65})_{4.0}Fe_{14}B$ ribbons are almost the same but lower, indicating that with the increase of the thickness of grain boundaries, the main phase grains are more segregated, and the

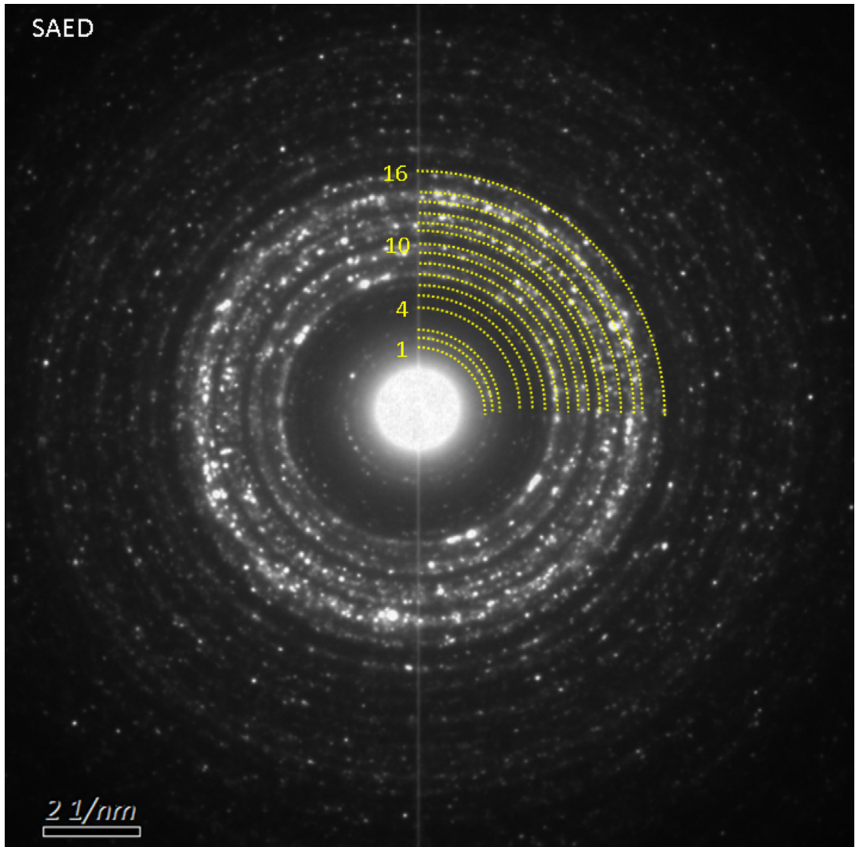

Measured			$(La,Ce)_2Fe_{14}B$			$CeFe_2$			La-Ce alloy		
No.	d (nm)	Int.	d (nm)	I/I0	hkl	d (nm)	I/I0	hkl	d (nm)	I/I0	hkl
1	0.710	w			101						
2	0.615	w			110						
3	0.555	w			111						
4	0.441	w			200						
5	0.395	w	0.392	10.9	210						
6	0.355	w	0.356	15.8	202						
7	0.327	m	0.330	41.1	212						
8	0.302	m							0.302	100	111
9	0.281	w	0.284	7.5	213						
10	0.271	s	0.270	57.4	311						
						0.258	66.3	220			
11	0.250	m	0.250	30.6	204						
12	0.240	s	0.241	78.1	214						
13	0.228	s	0.229	67.7	313						
						0.220	100	311			
14	0.213	s	0.213	100	410						
15	0.198	w	0.201	9.3	412						
16	0.189	m	0.188	25.2	413						

Fig. 4. Results of analysis of the SAED pattern of the $(La_{0.35}Ce_{0.65})_xFe_{14}B$ ribbon shown in this figure. In the table, I/I0 stands for the intensity, S stands for strong, M stands for medium, and W stands for weak.

effect of the difference in grain boundary thickness on intergrain exchange coupling becomes weaker.

4. Conclusions

In summary, high performance $(La_{0.35}Ce_{0.65})_xFe_{14}B$ ribbons, not only free of Tb and Dy, but also free of Pr and Nd, have been synthesized by melt-spinning method, which exhibit a well promising potential value in practical application. The compounds can crystallize in a tetragonal 2:14:1 structure in an appropriate wheel velocity range. The maximum magnetic energy product as high as 8.29 MGOe is achieved in $(La_{0.35}Ce_{0.65})_{2.4}Fe_{14}B$ ribbons, which were prepared at a wheel velocity of 20 m/s. Detailed analysis indicates that strong pinning effect dominates the

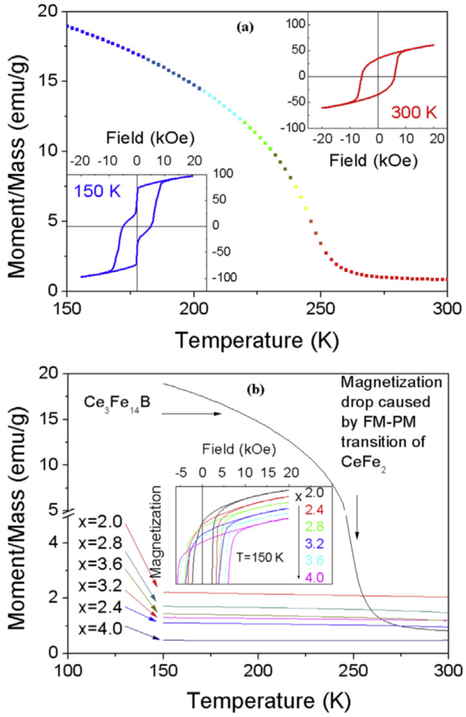

Fig. 5. The dependence of magnetization on temperature of (a) $Ce_{17}Fe_{78}B_6$ and (b) $(La_{0.35}Ce_{0.65})_xFe_{14}B$. The insets in (a) is the hysteresis loops of $Ce_{17}Fe_{78}B_6$ at 150 K and 300 K. The inset in (b) is the hysteresis loops of $(La_{0.35}Ce_{0.65})_xFe_{14}$ B at 150 K.

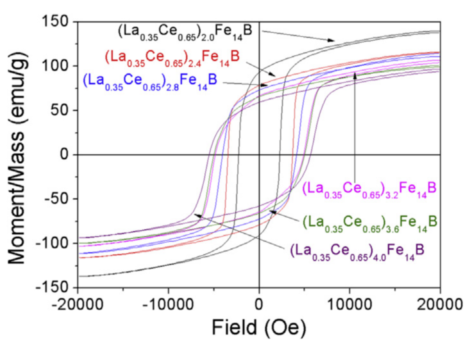

Fig. 6. The hysteresis loops of $(La_{0.35}Ce_{0.65})_xFe_{14}B$ ribbons prepared at a wheel velocity of 20 m/s.

Table 2
Room temperature magnetic properties of $(La_{0.35}Ce_{0.65})_xFe_{14}B$ ribbons.

Samples	Br kGs	Hcj kOe	$(BH)_{max}$ MGOe	Remanence ratio	Squareness
$(La_{0.35}Ce_{0.65})_{2.0}Fe_{14}B$	8.68	2.30	7.36	0.67	0.75
$(La_{0.35}Ce_{0.65})_{2.4}Fe_{14}B$	7.39	3.55	8.29	0.68	0.79
$(La_{0.35}Ce_{0.65})_{2.8}Fe_{14}B$	7.12	4.05	8.13	0.65	0.76
$(La_{0.35}Ce_{0.65})_{3.2}Fe_{14}B$	5.73	4.85	7.06	0.63	0.65
$(La_{0.35}Ce_{0.65})_{3.6}Fe_{14}B$	5.72	5.00	6.00	0.66	0.70
$(La_{0.35}Ce_{0.65})_{4.0}Fe_{14}B$	5.50	5.57	5.53	0.62	0.69

magnetization reversal process in all the rare-earth-rich ribbons, and the evidence of the existence of exchange coupling interaction was found. Industrial La–Ce mischmetal with impurities was used

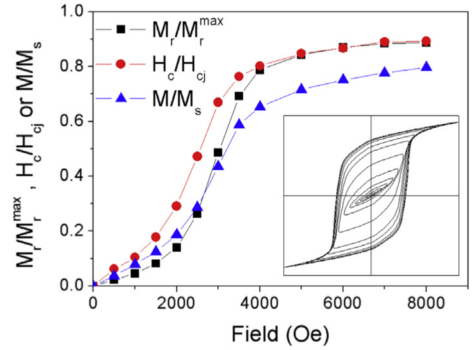

Fig. 7. The dependence of M, H_c and B_r on applied field in minor loops of $(La_{0.35}Ce_{0.65})_{2.4}Fe_{14}B$ ribbons.

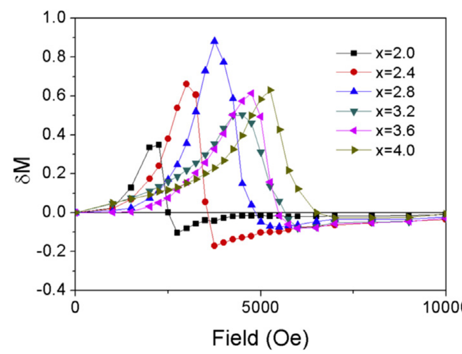

Fig. 8. The Henkel plots of $(La_{0.35}Ce_{0.65})_xFe_{14}B$ ribbons.

as the raw material, which makes the magnetic materials not only contribute to the resource leveling but also possess the advantage in cost of production.

Acknowledgments

This work was supported by the National Basic Research Program of China (Grant No. 2014CB643702).

References

[1] J.J. Croat, J.F. Herbst, R.W. Lee, F.E. Pinkerton, Appl. Phys. Lett. 44 (1984) 148–149.
[2] M. Sagawa, S. Fujimura, N. Togawa, H. Yamamoto, Y. Matsuura, J. Appl. Phys. 55 (1984) 2083–2087.
[3] C.D. Fuerst, T.W. Capehart, F.E. Pinkerton, J.F. Herbst, J. Magn. Magn. Mater 139 (1995) 359–363.
[4] J.M. Xu, Z.T. Sui, C.Z. Wang, J. Alloys Compd. 190 (1992) L9–L12.
[5] Z.B. Li, B.G. Shen, M. Zhang, F.X. Hu, J.R. Sun, J. Alloys Compd. 628 (2015) 325–328.
[6] C.J. Yan, S. Guo, R.J. Chen, D. Lee, A.R. Yan, J. Magn. Magn. Mater 50 (2014) 2102605.
[7] E. Niu, Z.A. Chen, G.A. Chen, Y.G. Zhao, J. Zhang, X.L. Rao, B.P. Hu, Z.X. Wang, J. Appl. Phys. 115 (2014) 113912.
[8] A.K. Pathak, M. Khan, K.A. Gschneidner Jr., R.W. McCallum, L. Zhou, K.w. Sun, K.W. Dennis, C. Zhou, F.E. Pinkerton, M.J. Kramer, V.K. Pecharsky, Adv. Mater 27 (2015) 2663–2667.
[9] J.F. Herbst, M.S. Meyer, F.E. Pinkerton, J. Appl. Phys. 111 (2012) 07A718.
[10] M.Y. Xing, J.Z. Han, Z. Lin, F.M. Wan, C. Li, S.Q. Liu, C.S. Wang, J.B. Yang, Y.C. Yang, J. Magn. Magn. Mater 331 (2013) 140–143.
[11] Eric J. Skoug, M.S. Meyer, F.E. Pinkerton, Misle M. Tessema, Daad Haddad, J.F. Herbst, J. Alloys Compd. 574 (2013) 552–555.
[12] N. Jones, Nature 472 (2011) 22–23.
[13] J.F. Herbst, Rev. Mod. Phys. 63 (1991) 819–898.
[14] P.E. Wohlfarth, J. Appl. Phys. 29 (1958) 595–596.
[15] Z.B. Li, M. Zhang, B.G. Shen, J.R. Sun, Appl. Phys. Lett. 102 (2013) 102405.